26th EPS Conf. on Contr. Fusion and Plasma Physics, Maastricht, 14 - 18 June 1999 ECA Vol.23J (1999) 597 - 600

Secondary generation of runaway electrons and its detection in tokamaks

I.M. Pankratov[1], R. Jaspers[2], K.H. Finken[3], I. Entrop[2]

1.Institute of Plasma Physics, NSC 'Kharkov Institute of Physics and Technology', Academicheskaya 1, 310108 Kharkov, Ukraine.
*2.FOM-Instituut voor Plasmafysica 'Rijnhuizen', Association EURATOM-FOM, P.O.Box 1207, 3430 BE Nieuwegein, The Netherlands**
*3.Institut für Plasmaphysik, Forschungszentrum Jülich GmbH, EURATOM association D-52425 Jülich, Germany**

1. Introduction

The secondary generation of runaway electrons is a fundamental physical phenomenon. Secondary generation is the process in which already existing high energy runaway electrons kick thermal electrons into the runaway region by close Coulomb collisions. The theoretical estimates of Sokolov [1] showed that if the confinement time of runaways is longer than this collision time an exponentially increasing runaway population develops (runaway avalanche). In 1993 the secondary runaway generation was first demonstrated in the TEXTOR experiment [2] in the steady state of low density ohmic discharges.

The avalanche process was recognized to dominate the runaway production during a major disruption in large tokamaks like ITER. The possible damage to the machine as a consequence of the local loss of the huge runaway population poses an important problem of a tokamak fusion reactor [3-5]. The runaway avalanche during disruptions was first demonstrated in TEXTOR [6].

The synchrotron radiation in TEXTOR is detected with an infrared (IR) camera (wavelength λ=3-8μm) for the **direct** observation of the runaway beam image. This diagnostic is used in TEXTOR to study the parameters of runaway electrons like beam size and position, number and maximum energy of runaways [7,8].

In the TEXTOR experiments it is found for both the steady state and disruptive phases of the discharge that the pitch angle $\theta=v_\perp/v_{//}$ is in the range 0.1-0.2 ($v_\perp$ and $v_{//}$ are the transverse and longitudinal velocities of the electrons with respect to the confining magnetic field). Note, that in Ref. [4] θ was underestimated to be $\theta>0.03$ for the disruption, but a more accurate estimate was given in Ref. [6]: $\theta\approx0.15$.

2. Secondary Generation

The electron motions in phase space ($p_\perp$,$p_{//}$) are described by Eqs. (1) and (2), $p_\perp$ and $p_{//}$ are the transverse and longitudinal momenta, Γ the relativistic factor:

$$\dot{p}_{//} = eE_{//}\left\{1-\left[1+\left(Z_{eff}+1\right)\Gamma^{-1}\right]p_{cr}^2\Gamma^2 p_{//}\left(p_{//}^2+p_\perp^2\right)^{-3/2}\right\}, \quad (1)$$

$$p_\perp \dot{p}_\perp = eE_{//}\,p_{cr}^2\Gamma^2 p^{-1}\left\{\left[1+\left(Z_{eff}+1\right)\Gamma^{-1}\right]p_{//}^2 p^{-2}-1\right\}. \quad (2)$$

Here $p_{cr}^2=4\pi e^3 m_e n_e L / E_{//}$, e and m_e are the charge and rest mass of the electron, L the Coulomb logarithm, Z_{eff} the effective ion charge and $E_{//}$ the inductive electric field.

In Fig. 1 the runaway region of electrons is shown ($\Gamma\approx1$). The straight lines $p_\perp=\sqrt{Z_{eff}+1}\,p_{//}$ are the places of points where $\dot{p}_\perp=0$. The curves $\dot{p}_{//}=0$ are notified by the letters a,b,c for different Z_{eff}. Their intersections are saddle points, S_a and S_r are the separatrices. Three cases are shown, Z_{eff}=3,6 and 40. Only electrons with initial positions ($p_{\perp0}$,$p_{//0}$) lying above the separatrix S_r will run away [9].

* Partner in the Trilateral Euregio Cluster

Initial positions of primary generated electrons are located along the $p_{//}$ axis ($p_{\perp 0} << p_{//0}$). Note that the initial positions of these may be even between the S_r and $\dot{p}_{//} = 0$ curves.

The secondary generated knocked out electrons have significant initial transverse momenta ($p_{\perp 0} >> p_{//0}$). They are arranged on elongated ellipses, the major axis of which is equal to the momentum of the incident high energy electrons. Two of these ellipses (curves 1,2) for different values of energy are shown in Fig. 1, with the assumption $\theta=0$ for the incident electrons.

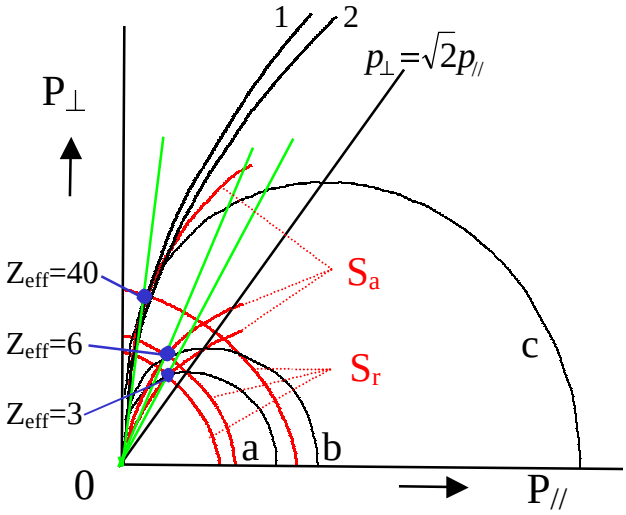

Fig. 1. The runaway region for different Z_{eff}.

If Z_{eff} is of the order or less than 10 the saddle point locates close to the maximum point $p_{\perp\max} = \sqrt[4]{12}\, p_{cr}\sqrt{Z_{eff}+2}/3$ in curves $\dot{p}_{//} = 0$ (like the curves a and b in Fig.1). These points $p_{\perp max}$ lie on the straight line $p_\perp = \sqrt{2}\, p_{//}$. That is why in this case the inequality of

$$p_\perp > p_{\perp cr} \quad , \quad p_{\perp cr} \approx p_{\perp\max} \tag{3}$$

determines the runaway region of the knocked out electrons [10]. Under these conditions it is possible to estimate the avalanching time by [11] (c the velocity of light):

$$t_0 \approx \sqrt{12} m_e c L (2 + Z_{eff})/9eE_{//} . \tag{4}$$

The dependence on Z_{eff} Eq. (4) was demonstrated experimentally in TEXTOR-94 [12].

Only if Z_{eff} is unrealistically large (curve c) the saddle point is sufficiently far from the maximum point in the curve $\dot{p}_{//} = 0$. In that case the dependence of Z_{eff} on $p_{\perp cr}$ and t_0 are not so strong as in Eqs. (3) and (4).

3. *Runaway generation and its detection in JET*

For relativistic electrons the instantaneous radius of curvature of the orbit R_{curv} is in good approximation given by:

$$R_{curv}^{-2} \approx R^{-2}[1 + \eta^2 + 2\eta\sin(\Theta + \alpha)] \tag{5}$$

and may oscillate strongly during the motion in a tokamak. Here $v_{//} >> v_\perp$, $\omega_{Bo}=eB_T/m_e c$ and

$$\eta = v_\perp / v_{dr}, \qquad v_{dr} = \Gamma v_{//}^2/\omega_{Bo} R, \tag{6}$$

R is the major radius of the magnetic surface, v_{dr} is the drift velocity, Θ the poloidal angle corresponding to the position of the guiding centre, α the phase of the cyclotron gyration.

Using the Schwinger approach [13] and taking into account the features of the relativistic electron motion in a tokamak (motion along the magnetic field line, cyclotron gyration and vertical centrifugal drift) the spectral density of the emitted power was derived in Ref. [14].

For the large parameter ξ:

$$\xi = \frac{4\pi}{3}\frac{R}{\lambda\Gamma^3}\frac{1}{\sqrt{1+\eta^2}} >> 1 \tag{7}$$

it is given by ($\Gamma >> 1$):

$$P(\lambda) \approx \pi c e^2 \sqrt{\frac{2\sqrt{1+\eta^2}}{\lambda^5 R\Gamma}} \left[I_0(a) + \frac{4\eta}{1+\eta^2} I_1(a) \right] \exp(-\xi), \qquad (8)$$

where $I_{0,1}(a)$ is the modified Bessel function and $a=(4\pi/3)\,(R/\lambda\Gamma^3)\,(\eta/(1+\eta^2)^{3/2})$. At

$$\lambda_m \approx \frac{8\pi}{15} \frac{R}{\sqrt{1+\eta^2}} \frac{1}{\Gamma^3}, \qquad (a(\lambda_m) \le 1.25) \qquad (9)$$

the $P(\lambda)$ expression takes a maximum value

$$P(\lambda_m) \approx 0.1 c e^2 (1+\eta^2)^{3/2} \Gamma^7 / R^3. \qquad (10)$$

The spectrum is shifted to smaller wavelengths compared with the case $\eta=0$ (see also Ref. [7]). Note that for $\eta^2>>1$ the parameter ξ is proportional to Γ^{-2} rather than to Γ^{-3} as in the case $\eta^2<<1$. Eq. (8) may be used for the case $\lambda<\lambda_m$. But for the case $\lambda>\lambda_m$, when $\xi \sim 1$ it is necessary to use the general expression (15) from Ref. [14] or for $\eta^2>>1$ the well known Schwinger expression (II.16) from Ref. [13] with $R_{curv} \approx \Gamma v_{//}^2 / v_\perp \omega_{B0}$.

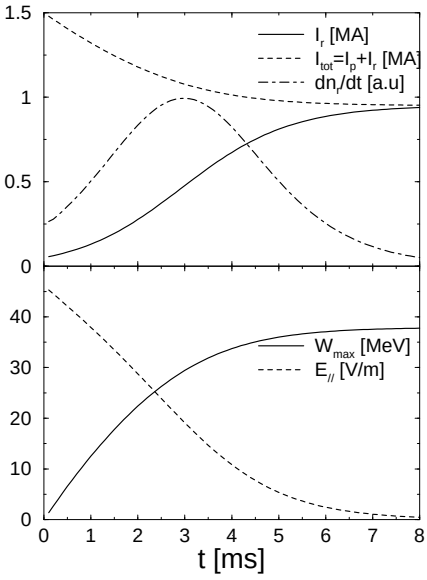

Fig.2: Simulation of time evolution of runaways in JET disruption 42155.

For diagnostical applications it is neccesary to predict the wavelength range of maximum emission. For the case of JET, one specific disruption (#42155) was analyzed, where a runaway beam was observed with soft X-ray cameras [15]. The runaways were first generated with a delay of (4-5)ms after the thermal quench. Then 6 ms after this start of this formation a runaway current plateau of $I_r \approx 1$ MA with a maximum electron energy of $W_{max} \approx 35$ MeV was observed.

In our analysis the (4-5) ms delay is attributed to the change of conditions of runaway production and confinement, and the acceleration of a primary runaway population to an energy in excess of 10 MeV, from which on the secondary generation becomes noticeable. Assuming that after this delay a primary runaway beam of $I_r=50$ kA (compared to the plasma current of 2MA) exists, we can calculate the time evolution $I_r(t)$, $E_{//}(t)$, $W_{max}(t)$ and the runaway production rate. These calculations are performed using the model of Ref. [4] and the results are shown in Fig. 2. In our calculation t=0 is the moment of the start of the secondary generation ($I_{tot} \approx 1.5$ MA). We assume that the plasma conductivity does not change appreciably after this time, hence the electric field is given by:

$$E_{//}(t) \approx E_{//}(0)\left[I_{tot}(t) - I_r(t)\right] / I_p(0). \qquad (11)$$

The total current is calculated according to $dI_{tot}/dt = -2\pi c^2 R E_{//}(t)/L_{int}$, $L_{int}=4.5\mu$H the JET internal inductance and $E_{//}(0)=45$ V/m, as quoted in Ref. [15]. For $I_r(t)$ primary and seconday generation (parametrized by t_0, Eq. (4), with $Z_{eff}=4$) are taken into account. The calculated $E_{//}$, I_r and W_{max} as well as the time development are remarkably close to the experimental observations. This important conclusion that the enhanced rate of secondary generation strongly reduces the time during which $E_{//}$ is high and hence the runaway production is high, was first shown in Ref. [4] and observed in TEXTOR [6]. Without taking the secondary generation into account under the in Ref. [15] quoted conditions, I_r would be at least 2 orders of magnitude lower.

For the calculated energy distribution function the synchrotron spectrum is presented in Fig. 3 for θ=0.05, 0.1 and 0.2. The next conclusions can be drawn from Fig. 3: a) the wavelength range where the maximum in emission occurs is around 3 μm and measurements should thus be made in this mid IR range and b) The synchrotron emission is two orders of magnitude higher than blackbody radiation from material structures inside the vessel or bremsstrahlung emission from the plasma in the investigated wavelength region. Runaway currents in excess of 10 kA will already dominate the IR emission. Further, the sharp low wavelength slope might explain why synchrotron radiation is not likely to be observed in the visible.

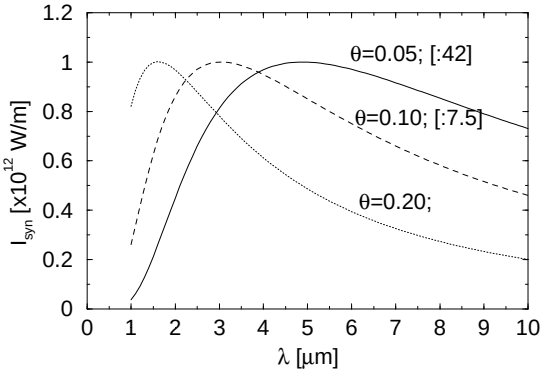

Fig. 3: Calculated synchrotron spectrum at 6 ms.

4. Conclusions

The evolution of the runaway parameters strongly influence the avalanching process. The large peak in the knocked out electron distribution function at low energies (see, e.g. [10,11]) which appears during the time when $E_{//}$ is very high (or Z_{eff} small), will then be below the separatrix S_r later, when $E_{//}$ strongly (>10 times) drops (or Z_{eff} strongly increases). Moreover, as a result of the $E_{//}$ drop (Z_{eff} increase) the runaway region and the production rate decrease and hence the runaway avalanche is drastically reduced.

Modelling of a JET disruption showed that here the secondary generation of runaway electrons plays an important role and leads to a runaway avalanche.

The IR diagnostic as used on TEXTOR-94 is well suited to diagnose the runaway electrons on larger machines like JET in the wavelength range λ=(1-5) μm.

Acknowledgements-Part of this work was carried out in the frame of the WTZ project UKR-014-97 between Germany and Ukraine. The authors also want to thank Dr. R. Gill from JET for providing the JET data.

References

1. Y.A. Sokolov, JETP Lett **29** (1979) 218.
2. R. Jaspers et al. , Nucl. Fusion **33** (1993) 1775.
3. R. Jayakumar, H.H. Fleischmann, S.J. Zweben, Phys. Lett. **A172** (1993) 447.
4. R. Jaspers et al., Nucl. Fuson **36** (1996) 367.
5. S. Putvinski et al., Plasma Phys. Control. Fusion **39** (1997) B157.
6. R. Jaspers et al., Proc. 25th EPS Conf. on Control. Fusion and Plasma Physics, Praha 1998, Vol. **22C**, 683.
7. K.H. Finken et al. , Nucl. Fusion **30** (1990) 859.
8. R. Jaspers, Relativistic runaway electrons in tokamak plasmas, PhD Thesis, Tech. University Eindhoven, The Netherlands, 1995.
9. V. Fuchs et al., Phys. Fluids **29** (1986) 2931.
10. N.T. Besedin, I.M Pankratov, Nucl. Fusion **26** (1986) 807.
11. I.M. Pankratov, N.T. Besedin, 23rd EPS conf. on Contr. Fus. and Plasma Phys., Kiev 1996, Vol **20C**, I-279.
12. I.M. Pankratov et al., Nucl. Fusion **38** (1998) 279.
13. J. Schwinger, Phys. Rev. **75** (1949) 1912.
14. I.M. Pankratov, Plasma Phys. Rep. **25** (1999) 165.
15. R.D. Gill et al., submitted to Nuclear Fusion, also JET P99-13.